Biomaterials 77 (2016) 320–335

Contents lists available at ScienceDirect

Biomaterials

journal homepage: www.elsevier.com/locate/biomaterials

Orthotopic transplantation of a tissue engineered diaphragm in rats

Elena A. Gubareva [a], Sebastian Sjöqvist [b], Irina V. Gilevich [a], Alexander S. Sotnichenko [a], Elena V. Kuevda [a], Mei Ling Lim [b], Neus Feliu [b], Greg Lemon [b], Konstantin A. Danilenko [a], Ramazan Z. Nakokhov [a], Ivan S. Gumenyuk [a], Timofei E. Grigoriev [c], Sergey V. Krasheninnikov [c], Alexander G. Pokhotko [d], Alexander A. Basov [e], Stepan S. Dzhimak [e], Ylva Gustafsson [b], Geoanna Bautista [f], Antonio Beltrán Rodríguez [b], Vladimir M. Pokrovsky [d], Philipp Jungebluth [b], Sergei N. Chvalun [c], Mark J. Holterman [g], Doris A. Taylor [h], Paolo Macchiarini [a, b, *]

[a] International Research, Clinical and Education Center of Regenerative Medicine, Kuban State Medical University, Krasnodar, Russian Federation
[b] Advanced Center for Translational Regenerative Medicine (ACTREM), Department of Clinical Science, Intervention and Technology (CLINTEC), Division of Ear, Nose and Throat, Karolinska Institutet, Stockholm, Sweden
[c] National Research Centre "Kurchatov Institute" (NRC "Kurchatov Institute") Laboratory of Polymer Materials, Moscow, Russian Federation
[d] Department of Human Physiology, Kuban State Medical University, Krasnodar, Russian Federation
[e] Common Use Center for Diagnostics of Nanomaterials, Structure and Properties, Kuban State University, Krasnodar, Russian Federation
[f] College of Medicine, University of Illinois, Chicago, IL, United States
[g] Department of Surgery, College of Medicine, University of Illinois, Chicago, IL, United States
[h] Texas Heart Institute, Center for Regenerative Medicine, Houston, TX, United States

ARTICLE INFO

Article history:
Received 8 July 2015
Received in revised form
1 November 2015
Accepted 6 November 2015
Available online 14 November 2015

Keywords:
Tissue engineering
Scaffolds
Diaphragm
Transplantation
Biocompatibility

ABSTRACT

The currently available surgical options to repair the diaphragm are associated with significant risks of defect recurrence, lack of growth potential and restored functionality. A tissue engineered diaphragm has the potential to improve surgical outcomes for patients with congenital or acquired disorders. Here we show that decellularized diaphragmatic tissue reseeded with bone marrow mesenchymal stromal cells (BM-MSCs) facilitates *in situ* regeneration of functional tissue. A novel bioreactor, using simultaneous perfusion and agitation, was used to rapidly decellularize rat diaphragms. The scaffolds retained architecture and mechanical properties and supported cell adhesion, proliferation and differentiation. Biocompatibility was further confirmed *in vitro* and *in vivo*. We replaced 80% of the left hemidiaphragm with reseeded diaphragmatic scaffolds. After three weeks, transplanted animals gained 32% weight, showed myography, spirometry parameters, and histological evaluations similar to native rats. In conclusion, our study suggested that reseeded decellularized diaphragmatic tissue appears to be a promising option for patients in need of diaphragmatic reconstruction.

1. Introduction

The diaphragm has multiple functions, most critically, its role in respiration. Its contraction flattens the dome-shaped diaphragm and central tendon, thereby increasing the volume of the thoracic cavity, reducing thoracic pressure and allowing air to flow into the lungs. Besides respiration, it also plays a role in swallowing and emesis, and serves as a barrier between the thoracic and abdominal cavities [1,2]. The diaphragm's importance is dramatically underscored in several congenital and acquired diseases. For instance, congenital diaphragmatic hernias (CDH) are relatively common birth defects (1:2500) caused by a malformation, or hole, in the diaphragm [3,4]. These defects can vary in size (from less than a centimeter to near total absence) and location [4] *i.e.* postero-lateral, anterior or central tendon. The vast majority (90%) of CDH occur in the postero-lateral diaphragm (*e.g.* Bochdalek hernia) [5,6]. Postero-lateral defects predominantly occur in the left hemi-diaphragm [5] and are commonly associated with lung

* Corresponding author. Advanced Center for Translational Regenerative Medicine (ACTREM), Division of Ear, Nose and Throat (CLINTEC), Karolinska Institutet, Hälsovägen 7, Plan 6, Huddinge, SE-141 86 Stockholm, Sweden.
E-mail address: paolo.macchiarini@ki.se (P. Macchiarini).

http://dx.doi.org/10.1016/j.biomaterials.2015.11.020
0142-9612/

hypoplasia due to *in utero* herniation of abdominal contents into the posterior thoracic space. This results in an underdeveloped lung, respiratory insufficiency and persistent pulmonary hypertension at birth. Despite advances in prenatal diagnosis and fetal treatments, this defect is still associated with high morbidity and mortality [6]. For infants who survive surgical repair, chronic respiratory insufficiency and neurodevelopmental problems are common. Outside the neonatal period, diaphragmatic insufficiency is usually caused by congenital myopathies, *e.g.* Duchenne muscular dystrophy [7], blunt or traumatic injury [8,9], idiopathic dysfunction [7] or, rarely, tumors [10].

A variety of open and minimally invasive surgical techniques have been described for diaphragmatic repair and reconstruction, both in children and adults. Unfortunately, surgical repair using natural or artificial patches is associated with a high rate of defect recurrence and significant morbidity and mortality [11,12]. When using autologous muscle flaps, they are likely to become atrophic while biological scaffolds (*e.g.*, bovine fascia lata and pericardium, human lyophilized dura, acellular sheet of porcine dermal collagen [13–15]) have incomplete muscular ingrowth and commonly suffer from defect recurrence [16,17]. Non-biodegradable synthetic materials (*e.g.* polytetrafluoroethylene or polypropylene mesh) tend to deform, leading to recurrent hernias and are associated with an increased incidence of bowel adhesion and obstruction [17]. A tissue engineering approach, where a biological scaffold is used to replace or repair diaphragmatic defects and reestablish function, could eliminate the need to utilize inadequate autologous replacement tissues or to implant synthetic, non-viable materials [17]. Such scaffolds could be available on demand, and would likely decrease morbidity and mortality [18,19]. The use of a scaffold and cells to create a tissue engineered diaphragm replacement will play a particularly vital role in the management of unique congenital anomalies in pediatric patients due to their high regenerative capacity and rapid growth. Based on the previous studies using acellular diaphragms and myoblasts [20], we investigated the orthotopic transplantation of diaphragmatic decellularized tissue re-seeded with BM-MSCs to evaluate feasibility and functional outcome.

Tissue engineering is an interdisciplinary field, applying the principles of cell transplantation, materials science and engineering to develop organ and tissue replacements that establish or restore native physiological function. One of tissue engineering's main principles is the use of a naturally or artificially derived three-dimensional scaffold on which to generate a nascent tissue. An ideal scaffold: *i*) encourages cell adherence and supports ingrowth, *ii*) exhibits mechanical properties of the target tissue, *iii*) supports angiogenesis and *neo*-vascularization for appropriate tissue perfusion, and *iv*) remains non-immunogenic to avoid graft rejection without the use of systemic immunosuppression. In our hands, creating a suitable biologically derived scaffold begins with decellularization of a donor organ or tissue. Decellularization uses physical or chemical means to eliminate immunogenic cells and cellular components, while preserving the native ultrastructure and composition of the extracellular matrix (ECM), thereby maintaining the biomechanical properties of the original organ. The optimal decellularization method varies depending on the tissue/organ. Based on previous pre-clinical and clinical experiences with tissue engineered airways [21–24] and esophagus [25] we have determined an ideal method to produce a biological diaphragmatic graft [26]. We here demonstrate that the tissue engineered diaphragms possess functional and regenerative capacity both *in vitro* and *in vivo* in a small animal model (Fig. 1).

2. Materials and methods

2.1. Animal care and use

A total of 97, eight-week-old male Lewis rats, weighing 250 ± 50 g (Rappolovo, Saint Petersburg, Russia), were used to complete the study, after approval by the Kuban Medical University Ethical Committees (Registration number 21/1, Krasnodar, Russian Federation) [27]. Animals were treated in compliance with the "Principles of laboratory animal care" formulated by the National Society for Medical Research, 2001, USA, and the "Guide for the care and use of laboratory animals" prepared by the Institute of Laboratory Animal Resources, National Research Council, and published by the National Academy Press, revised 1996, USA. The study overview is depicted in Fig. 1. Donor rats were euthanized *via* intraperitoneal barbiturate overdose of 150 mg kg^{-1}. The entire (costal and crural) diaphragms with connective tissue were isolated from the surrounding tissues, with careful preservation of their vascular supply. Explanted diaphragms were placed in cold Dulbecco's Phosphate Buffered Saline (PBS) (Gibco, Life Technologies, USA) with 1% antibiotics-antimycotics (Gibco, Life Technologies, USA) and stored at 4 °C for less than 24 h.

2.2. Diaphragm decellularization

The harvested diaphragm was dissected free from surrounding adipose tissue. The abdominal or subphrenic aspect of the vena cava was cannulated with a 22 G intravenous catheter (Terumo, USA) two centimeters below the right atrium and flushed with sterile PBS (Gibco, Life Technologies, USA) while its entrance into the right atrium was ligated. The organ was fixed to the cannulas using 6-0 prolene ligatures (Ethicon, USA) and mounted onto a customized bioreactor, designed to allow perfusion of the tissue but reduce excessive tension on the tissue during the process. In addition to standard agitation method [20], the diaphragm was simultaneously perfused at a rate of 6 ml min^{-1} retrograde through the vena cava into the right and left posterior (or caudalis) phrenic veins. The perfusate was eliminated *via* intramural branches of the *superior* and *inferior* phrenic arteries. Our previous detergent-enzymatic protocol [26] was adapted to consist of: 3 h 4% (w/v) sodium deoxycholate (Sigma Aldrich, USA), 10 min PBS (Gibco, Life Technologies, USA), 1 h DNase – I 2000 kunitz units (Sigma Aldrich, USA) diluted in PBS with calcium and magnesium (Invitrogen, Life Technologies, USA), and 2 washes of 30 min each of 2 mM EDTA (Sigma Aldrich, USA) in MilliQ water. Tissues were then rinsed for 12 h using PBS (Gibco, Life Technologies, USA). All steps were performed at room temperature, with a reagent final volume of 200 ml.

2.3. Histology

For histology, decellularized diaphragm was fixed overnight at room temperature in 10% neutral buffered formalin (Histolab, Sweden), processed and paraffin embedded. Samples were sectioned at 5 μm thickness. To evaluate the decellularization process and architecture, histological stains *i.e.* Hematoxylin and Eosin (H&E) (Histolab, Sweden), Masson's Trichrome (Sigma Aldrich, USA), and 4′,6-Diamidino-2-Phenylindole (DAPI) (Sigma Aldrich, USA) were performed according to manufacturers' instructions. To quantify fibrosis, van Gieson's staining (Sigma Aldrich, USA), was performed, and the area of fibrosis was analyzed using cellSens Entry Program (Olympus, Japan).

2.4. Ultrastructure

Decellularized diaphragms were incubated for 2 h in 2.5%

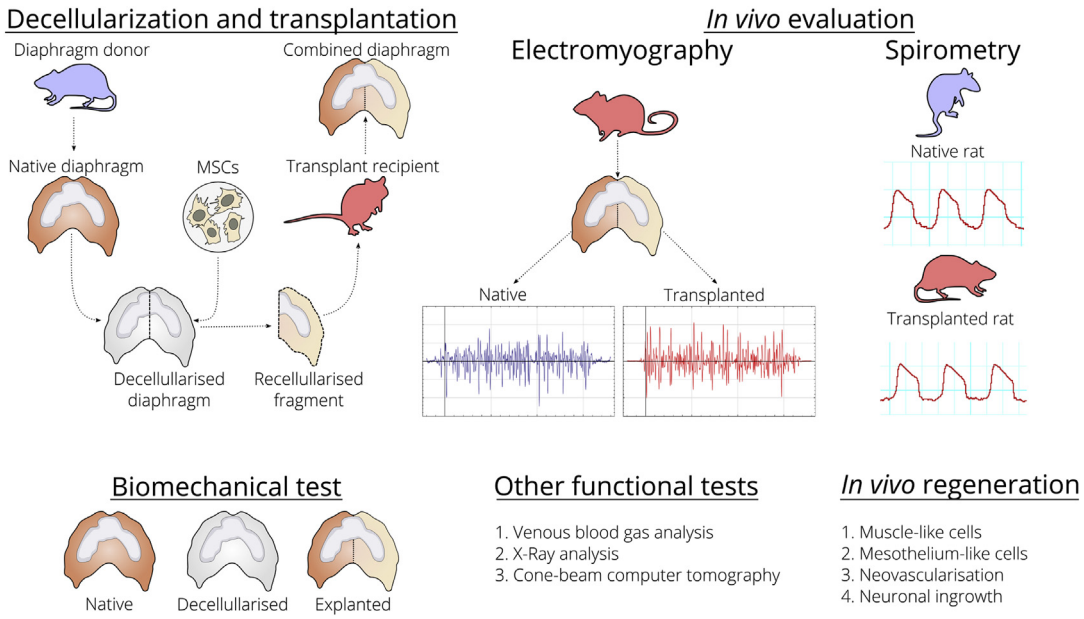

Fig. 1. Study overview. Donor diaphragms were decellularized in a customized bioreactor and subsequently recellularized with BM-MSCs. The reseeded tissue engineered grafts were transplanted into an orthotopic position in immunocompetent rats for three weeks. The strength and functionality of the tissues were tested biomechanically in parallel with transplanted and *in situ via* myography, spirometry and blood gas analyses. Anatomical data were acquired through X-ray and CT. The explanted grafts were further analyzed for *in vivo* regeneration of the essential diaphragm components: muscular-like, mesothelial-like and neuronal-like tissue, as well as *neo*-vascularization.

glutaraldehyde (Merck, USA) with 0.1 M cacodylate buffer (Prolabo, Sweden) at room temperature. Samples were then washed in cacodylate buffer and dehydrated through an ethanol gradient, processed through critical point drying, and sputter coated with gold before observation with a scanning electron microscope (JSM6490, Japan) to evaluate fiber configuration.

2.5. Immunohistochemistry

Paraffin sections were de-waxed and rehydrated by two changes of xylene for 15 and 5 min, followed by a sequential alcohol gradient for 6 min and rinsed in running tap water for 1 min. Antigen retrieval was performed with Rodent Decloaker (Biocare Medical, USA) for 40 min at 95–100 °C. The sections were cooled to room temperature for 20 min and blocked with Rodent Block R (Biocare Medical, USA) for 30 min at room temperature. The following primary antibodies were diluted in PBS at the respective concentrations: anti-laminin (1:100, ab11575, Abcam, UK), anti-elastin (1:50; ab21610, Abcam, UK), anti-fibronectin (1:100, ab6328, Abcam, UK), anti-collagen IV (1:100, ab6586, Abcam, UK), anti-collagen I (1:100, ab34710, Abcam, UK), anti-tropomyosin 1 (alpha) (1:100, ab77867, Abcam, UK); anti-cytokeratin 5 (1:100, ab34710, Abcam, UK), and anti-cytokeratin 18 (1:100, ab34710, Abcam, UK) and incubated overnight at 4 °C. The secondary antibodies were Mouse-on-Rat HRP Polymer (MRT621L, Biocare Medical, USA) and Rabbit on Rodent HRP-Polymer (RMR622, Biocare Medical, USA). For antibody and antigen reaction detection, Betazoid DAB Chromogen Kit (Biocare Medical, USA) was incubated for 3 min at room temperature. Samples were washed three times with PBS (Invitrogen, Sweden) between each step, counterstained with Mayer hematoxylin (Histolab, Sweden) and mounted with DPX mounting media (Sigma Aldrich, USA). For immunofluorescence, the following concentrations were used: anti-von Willebrand Factor conjugated FITC (1:100; ab8822, Abcam, UK), anti-MHC Class I conjugated FITC (1:20; ab22367, Abcam, UK), anti-MHC Class II (1:100, ab23990, Abcam, UK), anti-VEGF (1:200, ab46154, Abcam, UK), anti-desmin (1:200, ab15200, Abcam, UK), anti-actin (1:100, ab14128, Abcam, UK), anti-Ki67 (1:100, ab16667, Abcam, UK), anti-myoD1 (1:300, ab16148 Abcam, UK), and anti-β III tubulin (1:100, ab18207, Abcam, UK), then incubated overnight at 4 °C. For secondary antibodies, goat polyclonal secondary antibody to rabbit IgG – H&L (Alexa Fluor® 488, Life Technologies, NY, USA) (1:500, ab150077, Abcam, UK) and goat polyclonal secondary antibody to mouse IgG – H&L (Alexa Fluor® 555, Life Technologies, USA) (1:500, ab150118, Abcam, UK) were used and mounted with DAPI (Sigma Aldrich, USA). All sections were visualized using an inverted fluorescence microscope (Olympus IX51, Japan).

2.6. DNA isolation and quantification

Native and decellularized diaphragm samples were cut into pieces weighing approximately 20 mg each and placed in 1.5 ml microcentrifuge tubes. DNA was extracted and purified from the tissue using DNeasy Blood and Tissue Kit (Qiagen, Germany) according to the manufacturer's instructions. DNA concentration was measured on a spectrophotometer (Nanodrop, Saveen & Werner, Sweden) and normalized to blotted dry weight.

2.7. Pro- and antioxidant assay

Electron paramagnetic resonance (EPR) detects and identifies paramagnetic centers (PMC), the sources of which are odd-electron molecules, including free radicals. In this study we detected the semiquinone radical ($\bullet Q^-$) in tissues. Assessment of oxidative EPR state by spectral parameter measuring was carried out on a spectrometer (JEOL, JES FA 300, Japan) at 24 °C within the X range. The measured parameters included: super-high-frequency radiation with a capacity of 1 mW, microwave radiation with a frequency of 9144 MHz, and high frequency modulation amplitude of 0.1 mT. Both native and decellularized diaphragm samples were lyophilized in a vacuum freeze dryer "LS-1000" (Prointech, Russia Federation) and weighed (Ohaus scales, China, precision of balance ± 0.01 mg). EPR signal of a 30 mg sample was measured in a quartz vessel (5 mm in diameter). The concentration of paramagnetic

centers in the samples was evaluated by comparing each with the signal of the standard sample (TEMPOL, 4-hydroxy-2,2,6,6-tetramethylpiperidine 1-oxyl). Integral intensity of the signal in each sample was measured by double numerical integration.

To simultaneously quantify the antioxidant state, the ABEL® wide-range antioxidant test with Pholasin®, based on peroxynitrite usage (Microplate Test Kit ABEL-41M2, Knight Scientific Ltd, UK), was performed according to the manufacturer's recommendations. Briefly, prior to testing, 50 μl of 2 mg ml^{-1} SIN-1 (3-morphinolino-sydnonimine HCL, $C_6H_{10}N_4O_2 \cdot HCL$) was added to each well of a 96 well plate. Then, 100 μl assay buffer (control) or 95 μl assay buffer, 5 μl sample (native or decellularized) decellularized or native lyophilized and resuspended matrix was added, followed by 50 μl Pholasin®. Different concentrations of a vitamin E analog (VEA, Microplate Test Kit ABEL-41M2, Knight Scientific Ltd, UK) standard solution were used as a positive control. Fluostar Optima (BMGLabtech, Germany) was used to measure fluorescence intensity.

2.8. Subcutaneous implantation

To evaluate the immunological response *in vivo*, decellularized diaphragm samples were implanted under the dorsal skin. General anesthesia was administered with 5 U intramuscular injection of 2% Xylazin (Intervet, Netherlands), 3 U intramuscular injection of Zoletil 100 (Virbac, France) and 5 U subcutaneous injection of 0.1% Atropine Sulfate (LTD OZGSCDC, Kharkov, Ukraine). After ensuring adequate anesthesia, 1 cm diaphragm samples were implanted under the dorsal skin under sterile conditions. Three groups were compared: group 1: ($n = 3$) sham rats (dorsal incision made and closed without implantation of a sample), group 2: ($n = 3$) subcutaneous implantation of native diaphragm (1 cm sample of native muscular diaphragm implanted under the dorsal skin), and group 3: ($n = 3$) subcutaneous implantation of decellularized diaphragm (1 cm sample of decellularized diaphragm implanted under the dorsal skin). In groups 2 and 3, grafts were placed in a preformed subcutaneous space and all skin incisions were closed with interrupted 4-0 polypropylene (Prolene; Ethicon, USA) stitches. All animals were euthanized 7 days after implantation and were evaluated macro- and microscopically for immunological reaction. The diaphragm samples were excised with a 10 mm subcutaneous tissue margin, frozen in OCT (Histolab, Sweden), cryosectioned at 8 μm and stained for H&E.

2.9. Macrophage staining and visualization

Following excision from subcutaneous implantation, 8 μm cryosections per diaphragm ($n = 3$ per group) were stained for the macrophage marker CD68. Samples were fixed in 4% formaldehyde (Thermo Scientific, Cheshire, UK) for 10 min then blocked for 1 h at room temperature in Rat Background Blocker (MP-962-P100, A Menarini Diagnostics, Italy). Primary antibody CD68 (1 μg ml^{-1}; ab74704, Abcam, UK) was incubated overnight at 4 °C. Detection was performed with mouse specific HRP/DAB (ABC) Detection ICH Kit (ab64259, Abcam, UK). All slides were mounted using Consul-Mount (Thermo Scientific, UK) and were visualized using an inverted fluorescence microscope (Olympus IX51, Tokyo, Japan).

2.10. Bone marrow derived mesenchymal stromal cell isolation

Rat mesenchymal stromal cells (BM-MSCs) were obtained by flushing femur and tibiae with PBS (Gibco, Life technologies, NY, USA). The cells were collected and centrifuged at 300 *g* for 10 min. The pellet was suspended in cell culture medium consisting of DMEM low glucose, 10% fetal bovine serum and 1% antibiotic-antimycotic (Invitrogen, Life technologies, USA). The cells were seeded into a culture flask (BD, NJ, USA) at 37 °C in 5% CO_2 and culture medium was refreshed after 24 h to eliminate the non-adherent cells. The adherent fraction was cultured to 80% confluence. The isolated cells were characterized by flow cytometry and were stained positive for CD29, CD44, CD59, CD73, CD90, CD106 and negative for CD11b, CD31, CD45 markers as reported previously [28].

2.11. Cell viability on recellularized scaffolds

Cytocompatibility of decellularized diaphragms was evaluated by seeding rat BM-MSCs between passages 3 and 4 onto 6 mm discs of the scaffold. The discs were washed with PBS and 80,000 BM-MSCs were cultured for 50 h in 96-well plates (BD, USA). Unseeded discs were used as negative controls and cells seeded to tissue culture plastic (TCP) wells as positive controls. The samples were analyzed according to the manufacturer's protocol for cell viability with a colorimetric, 3-(4,5-dimethylthiazol-2-yl)-2,5-diphenyl tetrazolium bromide (MTT)-assay (Roche, Australia). Briefly, samples were incubated for 4 h at 37 °C with the MTT substrate followed by the addition of 10% sodium dodecyl sulfate (SDS) in 0.01 M HCl overnight at 37 °C. Subsequently, the supernatant was transferred to a new 96-well plate to measure the absorbency at 560 nm using a spectrophotometer (SpectraMax 250, Molecular Devices, USA). Live/Dead® Viability/Cytotoxicity Kits (Molecular Probes, Life Technologies, USA) were used according to the manufacturer's protocol to determine the cytotoxicity of the scaffold.

2.12. In vitro differentiation of recellularized scaffolds

Differentiation of rat BM-MSCS was investigated by identification of tissue-specific genes on the recellularized diaphragms. BM-MSCs were seeded at a cell density of 50,000 cells/cm^2 and analyzed after 3 weeks *in vitro*. RNA extraction was performed with the RNeasy Minikit and RNase free DNase kit (both Qiagen, Germany) to remove genomic DNA. High capacity cDNA Reverse Transcription kit (Applied Biosystems, Life Technologies, USA) was used to synthesize cDNA. The following TaqMan probes were used: CD90 (Rn00562048_m1), Desmin (Rn00574732_m1), Thy1 (Rn00562048_m1) and Myog (Rn01490689_g1). The housekeeping gene, GAPDH (Rn01775763_g1) was used as an endogenous control. All samples were analyzed on a Fast Real-Time PCR System 7500 (Applied Biosystems, Life Technologies, USA). Each sample set ($n = 3$) was run in triplicate, and water was used as a negative control. The expression levels for each sample were normalized to GAPDH and relative quantification of expression was estimated using the ΔΔCT method. The results are presented as relative fold change compared to cells grown in standard cultures on tissue culture plastic.

2.13. Real-time intracellular Ca^{2+} imaging assay

Decellularized diaphragms were cryosectioned at 25 μm ($n = 5$) and were placed on 35 mm cell culture plates (BD, NJ, USA). BM-MSCs were seeded onto the scaffold at a concentration of 50,000 cells/cm^2 and incubated at 37 °C for 3 weeks to induce spontaneous differentiation *in vitro*. Cells were then loaded with a Ca^{2+} specific dye Fluo-4 (Invitrogen, Sweden) at a concentration of 5 μM ml^{-1} and incubated at 37 °C for 30 min. After loading, cells were carefully rinsed with Krebs–Ringer's solution and kept in 2 ml of the same buffer. An upright wide field Ca^{2+} system observer (Zeiss, Germany) was used to record the Ca^{2+} transients and the cellular responses to agonists ATP (10 μM) and KCL (25 mM).

2.14. Recellularization of diaphragm for orthotopic transplantation

Decellularized samples measuring about approximately 1.5×2.5 cm^2 or 80% of the left hemi-diaphragm were treated with 70% ethanol for 15 min and washed twice with PBS with calcium and magnesium (Invitrogen, Life Technologies, USA), prior to cell seeding. The diaphragm samples were conditioned in 1 ml DMEM (Invitrogen, Life Technologies, USA) in 24 well plates for 24 h in a CO_2-incubator. The pieces were transferred to a new 24-well plate and 800 μl of cell suspension were pipetted onto the scaffolds. After 24 h the samples were transferred to a 6-well plate and 2 ml of media was added to each well. These scaffolds were cultured under static condition for 3 weeks at 37 °C in 5% CO_2 with media replacement every third day.

The number of BM-MSCs required for reseeding was calculated by determining the number of cells required to fully cover the surface of the diaphragm based on its surface area and the interfacial surface area of the attached cells. Hence the number of seeded cells, N_s, required to achieve 100% cell coverage, is given by: $N_s = A_d/A_a$, where A_d is the total surface area of the diaphragm and A_a is the average interfacial surface area of an attached cell. A typical value for the area of a decellularized diaphragm is $A_d = 9$ cm^2. The value $A_a = 281$ μm^2 was determined from image analysis of BM-MSCs attached to thin layers of electrospun PET/PU fibers [28,38]. Substituting these values into the equation gives $N_s = 3.2 \times 10^6$ cells as the number of cells required to reseed the diaphragm. The number of cells used for re-seeding was doubled, to compensate for loss due to cell death or cell detachment from the diaphragm during incubation.

2.15. Orthotopic transplantation

Fifteen adult male rats, weighing 250 ± 20 g each were used in this study. Operated animals were anesthetized with 5 U intramuscular injection of 2% Xylazin (Intervet, Netherlands), 3 U intramuscular injection of Zoletil 100 (Virbac, France) and 5 U subcutaneous injection of 0.1% Atropine Sulfate (LTD OZGSCDC, Kharkov, Ukraine). The rats were orally intubated with a 2.42 mm OD (1.67 ID) polyethylene catheter and ventilated with an Inspira small animal ventilator (Harvard Apparatus, USA) at 100 breaths min^{-1}. Rats were placed in a supine position and a left oblique subcostal laparotomy was made. Eighty percent of the left dome of the diaphragm was removed leaving only the pericostal aspects of the diaphragm. Three groups of animals were studied; group 1: control (normal, untreated $n = 5$), group 2: sham (resection of the left hemi-diaphragm and autologous re-implantation of the resected diaphragm $n = 5$), and group 3: treated (resection of the left hemi-diaphragm and replacement with tissue engineered reseeded scaffolds $n = 5$). Autologous diaphragm replacement or transplanted bioengineered recellularized diaphragm scaffolds were sutured to the native pericostal diaphragm remnant using an interrupted 6-0 monofilament polypropylene suture (Prolene; Ethicon, USA). The last suture was placed while the lungs were inflated to avoid pneumothorax. Laparotomy incisions were closed using two layers (fascia and skin) of interrupted 4-0 monofilament polypropylene suture (Ethicon, USA). The operation time was 40–50 min. The rats were breathing spontaneously immediately following the procedure and received a soft diet during the first 2 days. Animals were given one dose of antibiotic: 5% Baytril 0.2 ml kg^{-1} (Bayer Health Care, Russia) subcutaneous every day for the 5 days following transplantation. 21 days after surgery, the rats were euthanized with an intraperitoneal barbiturate overdose of 150 mg^{-1} before the diaphragm implants were harvested. The transplanted grafts or native diaphragm were excised, fixed in 10% neutral buffered formalin, and embedded in paraffin for analysis.

2.16. Pain and general health assessment scales

Post-operatively, animals were observed at 3 h, 12 h, 24 h and every 24 h thereafter for complications. The animals were allowed to consume food and water after the surgical procedure (but a soft diet for 2 days). A pain assessment scale [29] which uses changes in the animals' facial expressions was used. The scale has four categories including orbital tightening, nose/cheek flattening, ear changes and whisker changes [25]. Each category is evaluated as absent, moderate or obvious. We used the Karolinska Institutet health assessment checklist, which includes six additional categories: general condition, movements and posture, porphyrin staining, piloerection, respiration and skin integrity/wound healing [25].

2.17. Diaphragmatic electromyography

Electromyography (EMG) *in situ* was performed to detect and compare the electrical muscular activity on both sides of hemi-diaphragms *in situ*. Three groups were evaluated: native ($n = 2$, rats without surgery), sham ($n = 2$) and transplanted rats ($n = 2$) at the study-end point (21 days postoperatively). Animals were anesthetized (as described above) and a needle electrode was positioned, under sterile conditions, with the tip penetrating the studied diaphragms at two random points on both sides of the diaphragm, outside the central tendon regions. EMG potentials were acquired by NeuroBioLab (NeuroBioLab LTD, DL312AM-401, Russia) spectrum using the subtraction method. Signals were recorded with 10,000× amplification and filtered by the Notch filter to prevent AC interference – 20 dB of signal attenuation in the range of 49.7–50.3 Hz. All recordings were performed using a general PC with the software attached (Digiscope, NeuroBioLab LTD, Russia) by the hardware supplier. After the recordings, raw data was exported in plain text format for further analysis. The spectrum analysis and data visualization was performed using the software package GNU Octave.

2.18. Radiographic evaluations

Chest X-ray and cone-beam computed tomography (CT) was obtained on animals before ($n = 3$) and 21 days after ($n = 3$) transplantation. Chest X-rays were performed to compare the anatomical structure of both sides of the diaphragm and to detect any herniation of abdominal contents into the chest (Axion Icon R 200, Germany). Cone-beam CT was used to verify the absence of anatomical abnormalities after transplantation. CT was performed on a Rayscan Symphony V (Samsung Electronics, South Korea), which was selected because of its high resolution (0, 138 mm^3 voxel size) and low radiation intensity 36 μSv. Although this CT device was designed for dentistry and maxillofacial surgery, it was adapted for our purposes using a specially designed plate, made from non-radiopaque plastic. To accurately demonstrate structural differences detectable by CT imaging, rats were anesthetized, as previously described, and secured to the custom-made silicon stand.

2.19. Spirometry

Spirometry and flow–volume (F–V) curves were used to assess changes in respiratory function. Three groups were compared: group 1: native rats ($n = 5$), group 2: rats receiving sham surgery ($n = 5$), and group 3: rats receiving tissue engineered diaphragms ($n = 5$) using Spirometer Power Lab 8/35 (ADInstruments, Australia). Because the sensor of the spirometry module is very sensitive to any distortions, the system must be impermeable and without leaks; to achieve this and reduce dead space, special

isolation seals were designed and used. Rats were anesthetized using 5 U Xylazin 2% (Intervet, Netherlands) by intramuscular injection, 3 U Zoletil 100 (Virbac, France) by intramuscular injection and 5 U subcutaneous injection of 0.1% Atropine Sulfate (LTD OZGSCDC, Ukraine). All data were acquired by LabChart software (ADInstruments, Australia), designed specifically for recording and analyzing information from ADInstrument's hardware. All rats were secured in the prone position and were breathing on their own throughout the testing period. Each recording was made 1 min after fixation of the spirometry sensor to establish a baseline. Typical recording time was more than 120 s. The animals' vital signs were monitored during testing.

2.20. Blood gas analyses

Blood gas samples were collected 21 days post op and analyzed using a Radiometer ABL800 Flex (Radiometer Medical ApS, Denmark) to evaluate oxygenation and ventilation of native rats ($n = 5$), sham rats ($n = 5$) and rats transplanted with tissue engineered diaphragms ($n = 5$). Venous blood samples were obtained from rats' tail veins, heparinized, and then analyzed for hemoglobin (HHb), pH, partial venous pressures of oxygen (PvO_2) and carbon dioxide ($PvCO_2$), and oxygen venous saturation (sO_2) within 5 min of obtaining the samples.

2.21. Biotin assay

Biotin assay was performed to evaluate the function of the mesothelium as previously described [25,30], on four groups of samples: native ($n = 3$), decellularized ($n = 3$), mechanically damaged ($n = 3$) and explanted ($n = 3$). Briefly, Biotin (Long Arm) NHS (BioNordika, Sweden) was reconstituted to 1 mg ml^{-1} and applied to the mesothelium for one minute. Biotin does not penetrate into healthy epithelium due to crosslinking. The tissue was then washed three times for 5 min each in PBS, frozen in OCT, sectioned and stained according to the immunohistochemistry section. Detection was performed with mouse specific HRP/DAB (ABC) Detection ICH Kit (ab64259, Abcam, UK). All slides were mounted with Consul-Mount (Thermo Scientific, USA).

2.22. Neo-angiogenesis

In vivo neo-angiogenesis was evaluated with microscopic imaging 21 days after orthotopic transplantation. Samples of transplanted diaphragm were harvested, washed in PBS, fixed in 10% neutral buffered formalin solution overnight (Histolab, Sweden), processed and embedded in paraffin. Morphology was evaluated by staining for H&E (Histolab, Sweden), and neo-angiogenesis was confirmed by immunohistochemistry for VEGF and vWF.

2.23. Biomechanical tests

Two methods were used to generate a comprehensive biomechanical characterization of native, decellularized; and explanted tissue engineered diaphragms (21 days after orthotopic transplantation). All experiments were carried out using Instron 5965 (Instron, USA). Uniaxial deformation of five 20×10 mm^2 samples at a constant rate (10 mm min^{-1}) was studied to evaluate strength, deformation at break and apparent module at elongation of 20%. A cycling biaxial loading–unloading protocol analogous to the ASTM D5748 test was used to define long-term non-static mechanical resistance. The linear deformation of the diaphragm during spontaneous respiration was estimated on representative X-ray images using the Huygens approximation:

$$P = 2 \times l + 1/3 \times (2 \times l - L)$$

where l = AM – circular-arc segment; L = AB – chord of circle, AC = CB, CM – perpendicular to AB (Supplementary Fig. 1a and b). The diaphragm deformation was 8–10%, reaching a deformation rate of 200–300 mm min^{-1}, so that a peak deformation of 8% and deformation rate at 100 mm min^{-1} were chosen as test parameters. Samples were clamped in a ring frame with an inner diameter of 10 mm and loaded–unloaded 5000 times. A preload of 0.05 N was applied to minimize the heterogeneity of samples and strain field. Maximum displacement was 1.8 mm. Probe radius was 2 mm. Tests were performed in phosphate buffer at 30 °C. Three samples of each group were used to average the mechanical responses.

2.24. Statistical analysis

Results were expressed as mean ± standard deviation (SD). Wolfram|Alpha Pro (Wolfram Alpha LLC, USA), Wolfram Mathematica 9 (Wolfram Research, USA), and GraphPad Prism 6 (GraphPad Software, USA) were used for statistical analyses. All data were analyzed by analysis of variance (ANOVA) or Students *t*-test. The level of significance was indicated as follows: $^{*}P \leq 0.05$, $^{**}P \leq 0.01$.

3. Results

3.1. Diaphragm decellularization and scaffold characterization

During the decellularization, the diaphragms gradually turned translucent while the tissue dimensions remained unchanged (Fig. 2a, b). Histology of native diaphragms demonstrated the features of striated muscle tissue (transverse striations, large number of nuclei, and intrafibrous connective tissue) (Fig. 2c, e, g), whereas the decellularized diaphragms had no nuclei or muscle fibers but retained the general tissue orientation and architecture (Fig. 2d, f, h). Masson's trichrome staining revealed preservation of substantial amounts of collagen in the decellularized diaphragms in a similar configuration to native diaphragms (Fig. 2e, f). DNA staining confirmed the complete elimination of intact cell nuclei in the decellularized diaphragms compared to the native diaphragms (Fig. 2g, h). Scanning electron microscopy (SEM) showed a porous structure of the extracellular matrix (ECM) and presence of randomly arranged fibers, similar to native diaphragms (Fig. 2i, j). Immunohistochemistry of native and decellularized diaphragms revealed similar appearance of extracellular matrix proteins such as collagen I and IV, laminin, elastin, fibronectin and the angiogenic protein; vascular endothelial growth factor (VEGF) (Fig. 3a–l). The lack of intracellular proteins such as tropomyosin and von Willebrand factor (vWF) suggests the complete removal of larger cellular proteins (Fig. 3m–p).

Biomechanical characterization of both native and decellularized diaphragms was performed to determine if the decellularization process impacted the physical properties of the tissue. The stress–strain curves were similar in both native and decellularized groups (Fig. 4a), and were further subdivided into: *i*) elastic (reversible deformation) with linear stress–strain dependence (approximately up to $\varepsilon = 30\%$); *ii*) complex partial deformation – the curve deviates from linearity (elongation from 30 to 80%) with partially irreversible deformation; and *iii*) irreversible deformation, *i.e.* diaphragm starts to break (at $\varepsilon > 80\%$) (Table 1). To further characterize the mechanical properties, cyclical biaxial deformation was carried out using uniaxial tension protocol. After pre-loading, each diaphragm was cyclically loaded–unloaded while measuring displacement and force (Fig. 4b). Both native and decellularized

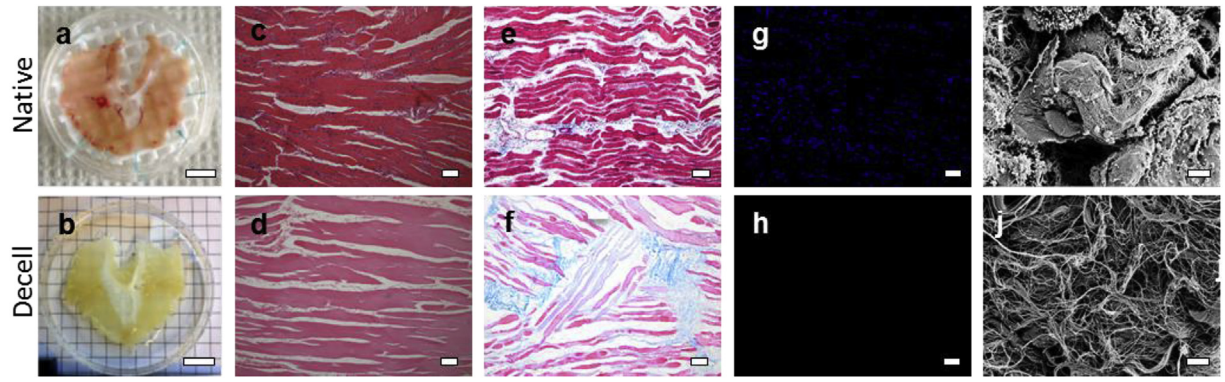

Fig. 2. Gross appearance and architectural evaluation of native and decellularized diaphragms. (**a**, **b**) Gross morphology of native (**a**) and decellularized (**b**) diaphragms (scale bar – 1 cm). (**c**–**f**) H&E staining shows muscle cells, cell nuclei in native (**c**) and an absence of cell nuclei in decellularized (**d**) diaphragms. Masson's trichrome staining demonstrated the presence of connective tissue fibers in native (**e**) and decellularized (**f**) diaphragms (scale bar–50 μm). (**g**–**h**) DAPI shows cell nuclei in native diaphragms (**g**), while no intact cell nuclei can be found in the decellularized tissue (**h**) (scale bar – 50 μm). (**i**–**j**) SEM evaluations of diaphragmatic surfaces before (native) (**i**) and after decellularization (**j**) (scale bar – 4 μm).

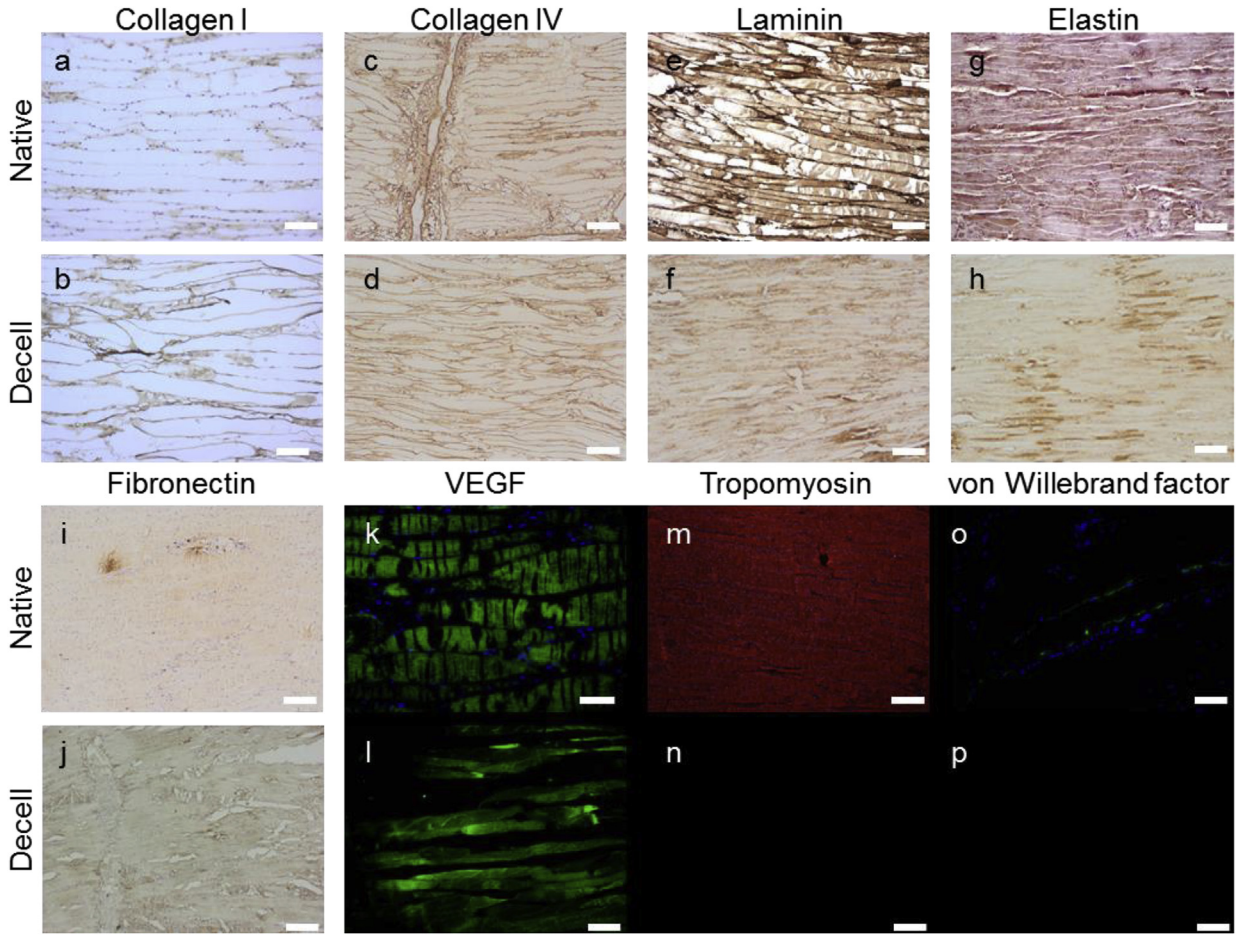

Fig. 3. Protein content. (**a**–**l**) The expression of collagen I and IV, laminin, elastin, fibronectin and VEGF in native (**a**, **c**, **e**, **g**, **i**, **k**) and decellularized (**b**, **d**, **f**, **h**, **j**, **l**) diaphragms, demonstrate retention of proteins. Expression of the intracellular contractile protein tropomyosin and endothelial marker vWF was present in native (**m**, **o**), but absent in decellularized (**n**, **p**) tissue (scale bar **a**–**j**, **m**, **n** – 50 μm, **k**, **l**, **o**, **p** – 20 μm).

groups demonstrated a comparable peak force of about 4–4.5 N. Within 10 min, or approximately 300 cycles, a substantial linear reduction of peak force to 2.5 N was observed in both native and decellularized diaphragms. After 10 min, the samples started to behave differently. Native diaphragms demonstrated constant peak forces at 2.0–2.2 N which reflects the long-term stability of native diaphragms. In contrast, decellularized diaphragms demonstrated a peak force at a level equivalent to native for approximately 1 h, or 1500 cycles, but, beyond this, the force diminished in a biphasic manner. Initially, the drop in force was dramatic, followed by a gradual reduction of peak force until the end of the experiment. The stress–strain curve results at various loading–unloading cycles

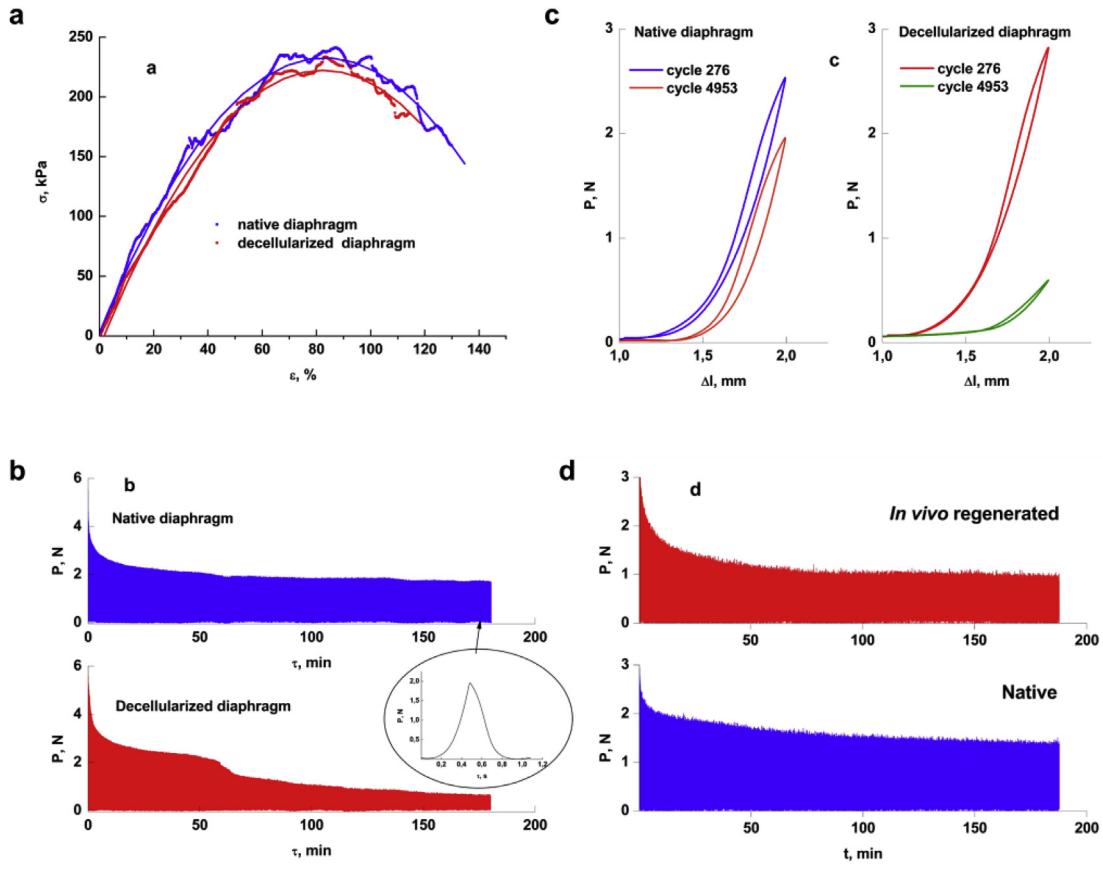

Fig. 4. Biomechanical properties. (**a**) Representative deformation curves during tensile testing of native and decellularized diaphragms. (**b**) Change in peak force in loading–unloading cycle of native and decellularized diaphragms during stress test. A representative cycle of native diaphragm loading–unloading (**b**, inset). (**c**) Representative loading–unloading cycles of native and decellularized diaphragms at the initial and final stages of stress test. (**d**) Change in peak force in loading–unloading cycle of native diaphragms and *in vivo* regenerated diaphragms.

Table 1
Biomechanical characteristics. Basic mechanical characteristics of diaphragm samples tested under uniaxial tension (σ_{max} – strength, ε_{peak} – deformation at peak, $E_{20\%}$ – apparent module at elongation of 20%).

Sample	σ_{max}, kPa	ε_{peak}, %	$E_{20\%}$, MPa
Native diaphragm	246 ± 21	85 ± 10	0.50 ± 0.05
Decellularized diaphragm	228 ± 38	81 ± 12	0.45 ± 0.08

(Fig. 4c) demonstrate a rubber-like response to this type of deformation in the native diaphragms (high initial deformation at low force followed by significant force increase with further extension). However, after approximately 5000 cycles, the decellularized diaphragms expanded at a low force, indicating a loss of its rubber-like response, which could be unfavorable for *in vivo* function during repetitive breathing movements. To determine if native mechanical properties were restored after *in vivo* regeneration, the same loading–unloading test was performed. Long-term mechanical results demonstrated that native and *in vivo* regenerated diaphragms had equal initial resistances and behave in a similar fashion throughout the study. However, the loss of durability at cyclic tests of native diaphragm is less than *in vivo*-regenerated scaffold, which could perhaps indicate a possible granulation of the *in vivo*-regenerated grafts (Fig. 4d).

3.2. Immunogenicity of decellularized scaffold

Since decellularized diaphragms have cellular components removed, we anticipated it would have a low immunologic profile. We evaluated for the presence of immunogenic elements and *in vitro* surrogates of immunogenicity and pro-inflammatory response. Lack of expected immunogenicity was confirmed by DNA quantification of the decellularized diaphragms. Approximately 74% of the nucleic acid content was removed from the diaphragm by the decellularization process (175.32 ± 46.92 ng mg^{-1} *vs.* 44.76 ± 23.25 S.D. ng mg^{-1} for decellularized samples) (****P < 0.0001) (Fig. 5a). Expression of the major histocompatibility complexes (MHC I and II), which elicit adverse host immune response *in vivo*, was also completely absent in the decellularized diaphragms (Fig. 5b–e). *In vitro* immunogenicity was evaluated by antioxidant testing and electron paramagnetic resonance spectroscopy. In comparison with native diaphragms, decellularized scaffolds had decreased antioxidant activity as demonstrated by earlier peak level, what correlated with low level of vitamin E (concentration 10 μM) (Fig. 5f). The results from spectral parameter readings by EPR showed that native diaphragms had a g-factor of 2.011 signal bandwidth (ΔH_{max}) from 324.8 to 326.5 mT and signal intensity (I) after conversion corresponded with the concentration of paramagnetic centers (PMC) and was 0.86 × 10^{-7} mol g^{-1} of lyophilized tissue (Fig. 5g). The decellularized diaphragms had a g-factor of 2.007, signal bandwidth (ΔH_{max}) is 0 mT, signal intensity (I) after conversion correlated with the concentration of PMC and lyophilized tissue did not contain PMC (Fig. 5h). These results suggest that there were no electron transport chains in the decellularized diaphragm samples, suggesting complete absence of

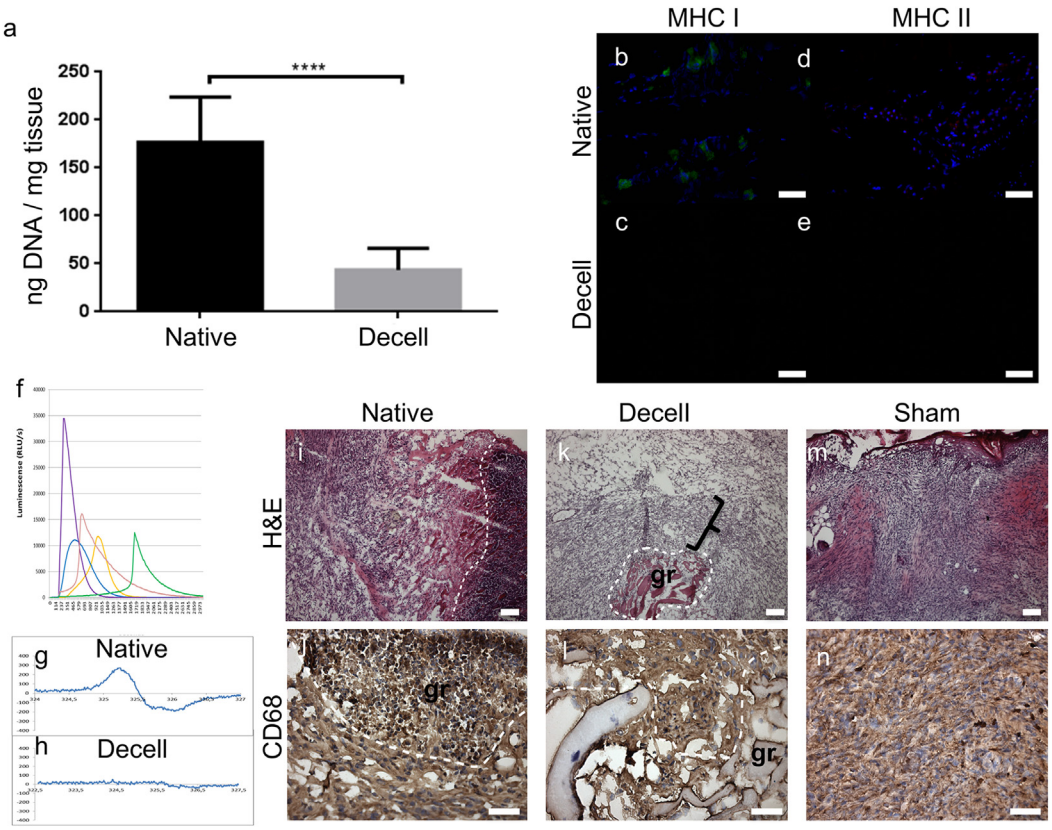

Fig. 5. Immunogenic properties of the scaffold. (**a**) DNA content in decellularized diaphragms was significantly lower than the native diaphragms (Student's *t*-test). (**b**–**e**) Major histocompatibility complexes I- and II-positive cells were present in native diaphragms (**b**, **d**) but absent in decellularized diaphragms (**c**, **e**) (scale bar – 20 μm). (**f**) Antioxidant activity was determined to assess antioxidant capacity of a sample. Antioxidants in native (yellow line) diaphragms gradually consumed the oxidants, delaying the time at which the maximum peak of light occurs in comparison with decellularized (blue line) diaphragms. Different concentrations of Vitamin E were used as positive control (purple – 10 μM, pink – 80 μM, green – 600 μM). (**g**–**h**) EPR spectroscopy of native (**g**) and decellularized (**h**) diaphragms. (**i**–**n**) H&E and CD68, a macrophage marker was stained after 7 days of subcutaneous transplantation: native (**i**, **j**), decellularized diaphragms (**k**, **l**) and sham surgery (**m**, **n**). The native diaphragms (**i**) were infiltrated with immune cells and fibroblasts and had distinct capsules (bracket) around the graft (gr), while the decellularized diaphragms were surrounded by fewer immune cells and had a thinner capsule (**k**, bracket). The sham surgery (**m**) showed similar inflammatory response to the decellularized group. (scale bar – 50 μm). Numbers of macrophages (brown staining) in native allotransplantation (**j**) were considerably higher compared with both decellularized organ (**l**) and sham surgery groups (**n**) (scale bar – 20 μm). (For interpretation of the references to color in this figure legend, the reader is referred to the web version of this article.)

viable cells.

After favorable *in vitro* results, *in vivo* immune reaction to diaphragm scaffolds were evaluated by subcutaneous heterotopic allotransplantation. Three groups were compared: group 1: sham (skin incision only) ($n = 3$), group 2: native allogeneic diaphragms ($n = 3$) and group 3: decellularized allogeneic diaphragms ($n = 3$). After 7 days, the native diaphragms elicited a severe immune response (Fig. 5i). However, the decellularized diaphragms (Fig. 5k) provoked a less severe lymphocytic inflammatory reaction, less surrounding tissue edema, and had thinner fibrous capsule formation similar to sham (Fig. 5m). Neither necrosis nor degradation of the decellularized grafts was observed (Fig. 5k). Macrophage marker CD68 demonstrated highest macrophage infiltration in the native group (Fig. 5j), which indicates a higher immunogenicity in comparison to the decellularized and sham group (Fig. 5l, n). There were no differences in the macrophage responses between the sham and decellularized groups, suggesting that the decellularized diaphragms did not elicit an increased immune response when compared to sham.

3.3. *In vitro analyses of recellularized scaffolds*

Allogeneic BM-MSCs were seeded onto decellularized diaphragms to evaluate cytocompatibility. Cell attachment was confirmed by H&E (Fig. 6a), 4′-6-diamindino-2-phenylindole (DAPI), SEM imaging (Fig. 6b, c) and cells were found proliferating based on a positive Ki-67 staining (Fig. 6d). After three weeks *in vitro*, cells were stained positive for both endothelial and muscular markers (VEGF, vWF, desmin) (Fig. 6e–g). 3-(4,5-dimethylthiazol-2-yl)-2,5-diphenyltetrazolium bromide (MTT) assay confirmed that the adherent cells were metabolically active at slightly lower levels than cells on tissue culture plate (TCP) (Fig. 6h). A Live/Dead assay indicated that the recellularized graft contained approximately 90% viable cells (Fig. 6i). Scaffold-induced differentiation was analyzed by comparing the tissue culture plate (TCP) cell cultures to the cells reseeded on decellularized diaphragms (Fig. 6j). We found a significant increase in gene expression for MSC-marker gene *CD90* ($^*P < 0.001$), a slightly decreased expression of muscular marker gene *desmin* and an absence of *Myog* were observed (Fig. 6j). Intracellular calcium transients were measured to assess spontaneous and induced Ca^{2+} fluctuations, as a surrogate for excitability, and were found to be negative for cells cultured on the scaffold for three weeks (data not shown). The cells also did not respond to stimulation with KCL and ATP at different concentrations. These results may suggest that three weeks after reseeding, the intracellular Ca^{2+} machinery [31] is still primitive and that full differentiation of cells on the decellularized diaphragm scaffold had not yet occurred. Contrary to this assumption, morphology changes

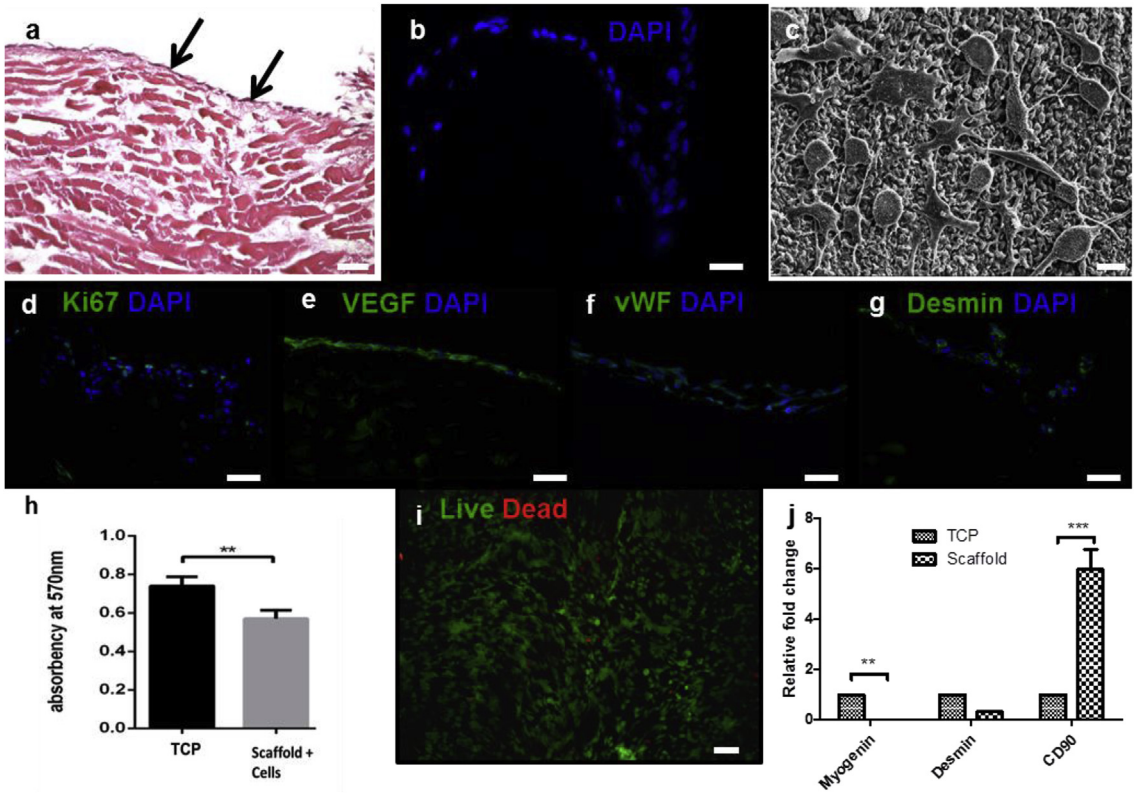

Fig. 6. Scaffold reseeding. BM-MSCs were seeded onto the decellularized diaphragms. Histological analysis after three weeks of culture shows cell adhesion by H&E (**a**) indicating adherent cells (**a**, arrows), DAPI staining (**b**) and SEM (**c**) (scale bar – 20 μm). (**d**) Ki-67 indicates that cells were proliferating. The reseeded diaphragms stained positive for VEGF, vWF and desmin (**e**–**g**) (scale bar – 20 μm). (**h**) MTT-assay after 48 h indicates viable and metabolically active cells on the scaffold (Student's *t*-test). (**i**) Live/Dead assay: approximately 90% of cells remained viable after 21 days of culture on the scaffold (scale bar – 50 μm). (**j**) Gene expression profiles of recellularized diaphragm demonstrated that majority of cells maintained *CD90* expression, had a slight down regulation for *desmin* and no expression for *myogenin*, when compared to the tissue culture plastic (TCP) (non-repeated, two-way ANOVA with Bonferroni post-test).

observed during this period suggest elongated myoblast-like cells.

3.4. Orthotopic transplantation and recovery

Under general anesthesia, 80% of the recipient's left dome of the diaphragm ($n = 5$) was removed and replaced with a recellularized graft (Fig. 7a, b), sutured to the residual pericostal diaphragmatic tissues (Fig. 7c). For comparison sham surgery ($n = 5$) was performed using the same surgical technique to remove 80% of the left diaphragm dome and use the same resected muscle tissues to restore it. Twenty-one days after surgery, transplanted grafts were without signs of infection or implant rejection, and the grafts were entirely integrated with the native diaphragm (Fig. 7d). During the 21 post-operative days, quality of life, pain parameters [29], general health scales and weight curves were measured, all of which suggested normal recovery and growth. During post-operative days 0–3, both transplanted and sham operated animals lost weight, reaching on average 84% and 82% respectively of their preoperative weight. The transplanted group reached their preoperative weight on day 9, while the sham group reached it at day 12–15. On day 21, the transplanted rats had caught up with unoperated rats, while the sham group still had a lower average weight (Fig. 7e). The animals demonstrated no clinical signs of herniation; infection or rejection and no mortality were observed during the study period of 21 days.

3.5. Functional outcomes

Spirometry revealed flow–volume loops with similar patterns for native, sham and transplanted rats (Fig. 7f) with no significant differences in respiratory rate and tidal volume between native ($n = 5$), sham ($n = 5$) and transplanted rats ($n = 5$). Additionally, blood gas analyses revealed no statistically significant difference in $PvCO_2$, PvO_2, pH, hemoglobin (Hb) and saturated oxygen (sO_2) levels between native and transplanted rats ($^*P < 0.05$) (Table 3). We observed significant differences between native and sham as well as between sham and transplanted: PvO_2, sO_2 and Hb level were lower in sham compared with native and transplanted rats ($^*P < 0.05$, $^{***}P < 0.001$) (Table 3). EMG was performed to assess the neurological conduction and muscle responses of the *neo*-diaphragm (Fig. 8a–l). Most of the spectral components of the signal are concentrated in a range of approximately 200–800 Hz. Different analyses (Table 2) were applied to the EMG data to quantify the difference between the signals from the two domes, in terms of characteristics such spectral content, temporal delay, signal range and signal root-mean-square (RMS) amplitude. The analyses revealed some marked differences between the groups in terms of the mean values of the comparison measures. However, except for the case of the signal amplitude comparison, there was no statistical significance between the results from the different groups. Hence, the signals in the operated and native domes can be considered to be similar. Computed Tomography (CT) and X-ray evaluations were used to assess the anatomic integrity of the tissue engineered constructs. On the CT scans (Fig. 9a–g), there were no signs of abdominal organ herniation into the left pleural cavity or signs of weakness at the site of the left dome implantation (eventration). Further, no signs of violation of its barrier function

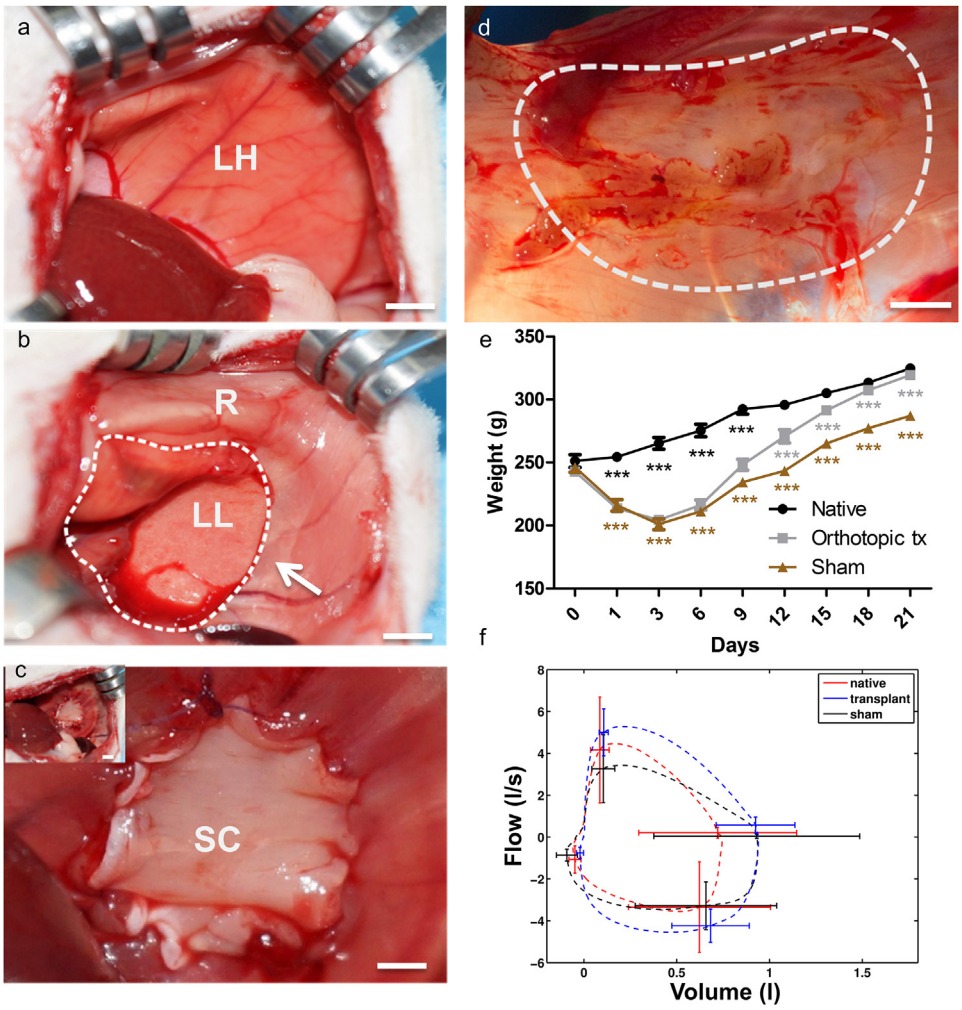

Fig. 7. Diaphragm transplantation. (**a**) Intact left dome of diaphragm (**LH** – left hemidiaphragm), (**b**) Diaphragmatic defect (marked by dashed line, **LL** – left lung), (**c**) Defect repaired by transplant with tissue engineered construct (**SC** – scaffold), (**d**) Implant (marked by dashed line) 21 days after surgery (scale bar– 0.5 cm). (**e**) Postoperative weight curves. The animals initially lost weight (up to 13.3% in the sham group), but all gained weight after 3–4 days. Weight gain was higher in the transplanted animals (*** indicates $P < 0.001$, *** Native *vs.* Orthotopic, ✻✻✻ Native *vs.* Sham, ✻✻✻ Orthotopic *vs.* Sham, error bars – SD, non-repeated, two-way ANOVA with Bonferroni post-test. n = 5 each) (**f**) Lung function evaluation – spirometry flow–volume graph of three experimental groups ($n = 5$, each) – native, transplanted and sham group. For each rat, an averaged flow rate–volume curve was obtained from the complete spirometry recording. For rats within the same group a mean curve (dashed) was calculated with error bars indicating the standard deviation ($n = 5$) of the location of corresponding points on the flow rate–volume curves for the different rats in the group.

(residual pneumothorax or pneumoperitoneum), signs of local inflammation such as free abdominal fluid, pleural effusion nor diaphragmatic-related lung dysfunction (atelectasis) were observed. The position of the heart remained normal and there was no bronchial or tracheal deviation or other organ displacement. Both sides of the diaphragm in the transplanted group had equal diaphragmatic excursion on X-ray, which suggested normal caudal and cephalad motion without paralysis (Supplementary video 1).

Supplementary video related to this article can be found online at http://dx.doi.org/10.1016/j.biomaterials.2015.11.020.

3.6. Post-mortem graft evaluation

All animals survived until the 21-day endpoint. The tissue engineered construct was well integrated into neighboring tissue and re-vascularization was confirmed by macroscopic observation (Fig. 10a). The grafts were then explanted with a margin of native tissue. Macroscopically, the explanted diaphragms looked similar to the native; normal post-operative inflammation was evident near the area of surgical anastomosis. In two cases, adhesions formed between the left liver lobe and the abdominal surface of the diaphragm, however, this did not affect the physiological function of the graft, based on the functional evaluations mentioned above (EMG, blood gas analyses *etc.*). H&E staining revealed several blood vessels surrounding the grafts (Fig. 10b), positive for vWF and VEGF (Fig. 10c–d). *In vivo* evidence of revascularization was provided by macroscopic observation of new vessel growth in and around the implanted tissue engineered organ (Fig. 10a, Supplementary video 2). Immunostaining for β-III-tubulin provided initial evidence for re-innervation of the graft (Fig. 10e). The presence of desmin, MyoD1 and actin-positive cells indicated muscle-like cells were present (Fig. 10f–h). MyoD1-positive cells were observed primarily on the periphery of the scaffold (Fig. 10g) whereas desmin and actin-positive cells completely covered the abdominal surface (Fig. 10f, h). Additionally, epithelial-like cells (cytokeratin 5 and 18-positive cells) were detected throughout the scaffold (Fig. 10i, j). All layers of the tissue engineered diaphragm graft contained proliferation marker Ki-67 positive cells (Fig. 10k). In the sham group, fibrotic changes of approximately 60% were identified by van Gieson's staining. The transplanted reseeded scaffold revealed the

Table 2
Quantitative comparison between EMG signals from the two domes of the diaphragm. The differences between the signals from the two domes in each group were quantified according to different signal characteristics. Results are reported as the mean and standard deviation of the number of values indicated.

	Native ($n = 3$)	Sham ($n = 3$)	Transplant ($n = 2$)
Spectral content[a]	0.15 ± 0.07	0.32 ± 0.12	0.27 ± 0.08
Temporal delay[b]	$(1.0 \pm 1.7) \times 10^{-4}$	−0.04 ± 0.15	$-(2.3 \pm 2.0) \times 10^{-3}$
Signal range[c]	0.55 ± 0.11*	1.44 ± 0.49*	1.04 ± 0.05
Signal RMS[d]	0.34 ± 0.04	0.31 ± 0.33	0.18 ± 0.12

[a] The amplitudes of the spectrogram components were normalized at each time point using the root mean square (RMS) of all the frequency components at that time, and the resulting values at each frequency were RMS-averaged over time. The absolute values of the differences between the resulting values from the two domes, divided by the values from the native dome, were then averaged over all frequencies.

[b] Cross correlation was applied to the signals from the two domes and the temporal delay (in seconds) was reported as the delay at which the value of the cross correlation was maximum.

[c] Reported as the ratio of the range of the signal (difference between the maximum and minimum value) in the operated dome to the range of the signal in the native dome.

[d] Reported as the absolute value of the difference between the RMS time-averaged signals in the operated and native domes, divided by the RMS-average of the signal in the native dome. (*P < 0.05).

Table 3
Venous blood gas analyses. The comparison of pH, blood gases ($PvCO_2$, PvO_2), hemoglobin (Hb) concentration and oxygen saturation (sO_2), in native, sham and transplanted animals at 21 days after surgery. Results presented are ±standard deviation, *P < 0.05, **P < 0.001.

	Native	Sham	Transplanted
pH	7.27 ± 0.03	7.34 ± 0.02	7.29 ± 0.04
$PvCO_2$, Torr	40.55 ± 4.1	49.06 ± 3.2	41.38 ± 3.5
PvO_2, Torr	74.68 ± 9.3*	49.42 ± 2.5	72.13 ± 7.2*
Hb, g l^{-1}	115.30 ± 8.5**	37.20 ± 14.9	93.67 ± 7.8**
sO_2, %	90.38 ± 3.3**	69.00 ± 3.9	90.58 ± 2.5**

presence of granulation tissue but not fibrosis. Desmin, Myod1, cytokeratin presenting cells, as well as newly formed vessels and nerve tissue progenitors were identified by immunohistochemistry. As previously described [25,30], the biotin assay was used for detection of an intact epithelium. Biotin does not penetrate through healthy epithelium, due to cross-linking of tight junction proteins. To confirm its inability to penetrate tight cell junctions, a native diaphragm was used as a positive control, where the biotin stained only the superficial mesothelium (Fig. 10l). When the diaphragm was damaged with a scalpel, biotin was detected in the muscular tissue, due to the absence of an impenetrable epithelial barrier (Fig. 10m). The explanted *in vivo* recellularized transplant stained in a similar manner to the native diaphragm (Fig. 10n), while the decellularized resembled the damaged diaphragm (Fig. 10o). This suggests that the recellularized transplant acquired barrier properties similar to the native tissue.

Supplementary video related to this article can be found online at http://dx.doi.org/10.1016/j.biomaterials.2015.11.020.

4. Discussion

Large diaphragmatic defects pose a significant surgical challenge. This problem is especially difficult for the repair of neonates with congenital diaphragmatic hernia. In some cases, the repair requires simple suture of the edges of the diaphragmatic defect, while larger defects require placement of natural tissue or artificial patches to close the defect. The resulting *neo*-diaphragm is not dynamic and therefore non-functional. In addition, it does not grow with a child and often pulls away from the growing chest wall resulting in hernia recurrences and the need for repeated repairs. This current suboptimal method has prompted investigation of the usefulness of regenerative medicine and tissue engineering strategies to create a dynamic and functional diaphragmatic replacement.

Successful creation of tissue engineered tissues and organs requires several key components including a scaffold similar in size and structure to the native organ or tissue needing repair [32]. Further, the scaffold should be non-immunogenic, have similar biomechanical properties to the native organ, support cell growth and induce angiogenesis. Decellularized diaphragms have the potential to provide each of these properties, while preserving the histo-architecture of the intact diaphragms including vascular architecture. The described gentle but rapid decellularization process did not only remove cellular components but provided an ECM with intact biomechanics.

Lack of immunogenicity of the decellularized diaphragms was confirmed by *in vitro* EPR spectroscopy, which demonstrated a complete absence of electron transport chains and reduced antioxidant activity. *In vivo* recipient immune response was evaluated by heterotopic transplantation of the scaffolds under the dorsal skin. After 7 days, limited adverse inflammatory response to the decellularized diaphragms was observed, including a significant reduction in the number of recruited macrophages, when compared to the focal cellular response elicited by the cell-containing native allo-implant. These findings imply minimal immunological activity of the ECM and indicate that the decellularized diaphragms were well tolerated by the host animal without the need for systemic immunosuppression, which is in line with previous preclinical tissue engineered implants [22,25].

After confirmation of non-immunogenicity, adult allogeneic BM-MSCs were used to recellularize the grafts. The primary advantages of this cell source are the ability to acquire a large number of autologous cells and their known immunomodulatory effects [33], previous successful experience from clinical transplantation of tissue engineered tracheae [34], their proven safety and the lack of controversy involving ethical issues which are associated with embryonic, induced pluripotent and tissue specific progenitor cell usage. Cell adherence to the scaffold and successful proliferation were demonstrated. The *in vitro* studies indicated that the decellularized grafts are cytocompatible, can be repopulated with stem cells and support early stage myogenic differentiation on protein level.

Evaluations of biomechanical properties of the decellularized diaphragms suggest that the decellularization process negatively impacts the scaffold, however, these effects are partially or completely reversed after successful recellularization of the scaffold. This evaluation included cyclic uniaxial deformation testing and a dynamic, loading–unloading to simulate physiologic breathing conditions. As expected, decellularized matrices had a tendency to be weaker and stiffer than their native counterparts likely due to the stretch of the macromolecular collagen network, resulting in diminished elasticity. However, testing of the explanted recellularized diaphragms showed return of rubber-like properties, similar to that of the native diaphragms. Return of these properties *in vivo* might be crucial for the long-term durability and functionality of the diaphragm replacement, and has been lacking in traditional natural or artificial diaphragm substitutes [14–16,18].

In vivo success of any tissue engineered organ also depends on its ability to promote *neo*-angiogenesis as re-vascularization is required for sufficient cellular repopulation [35]. *Neo*-angiogenesis also promotes migration of native proliferating cells within the damaged region. Angiogenic evaluation on orthotopically transplanted grafts after 21 days *in situ* was chosen because it corresponds to about one and a half year in humans [36] and represents

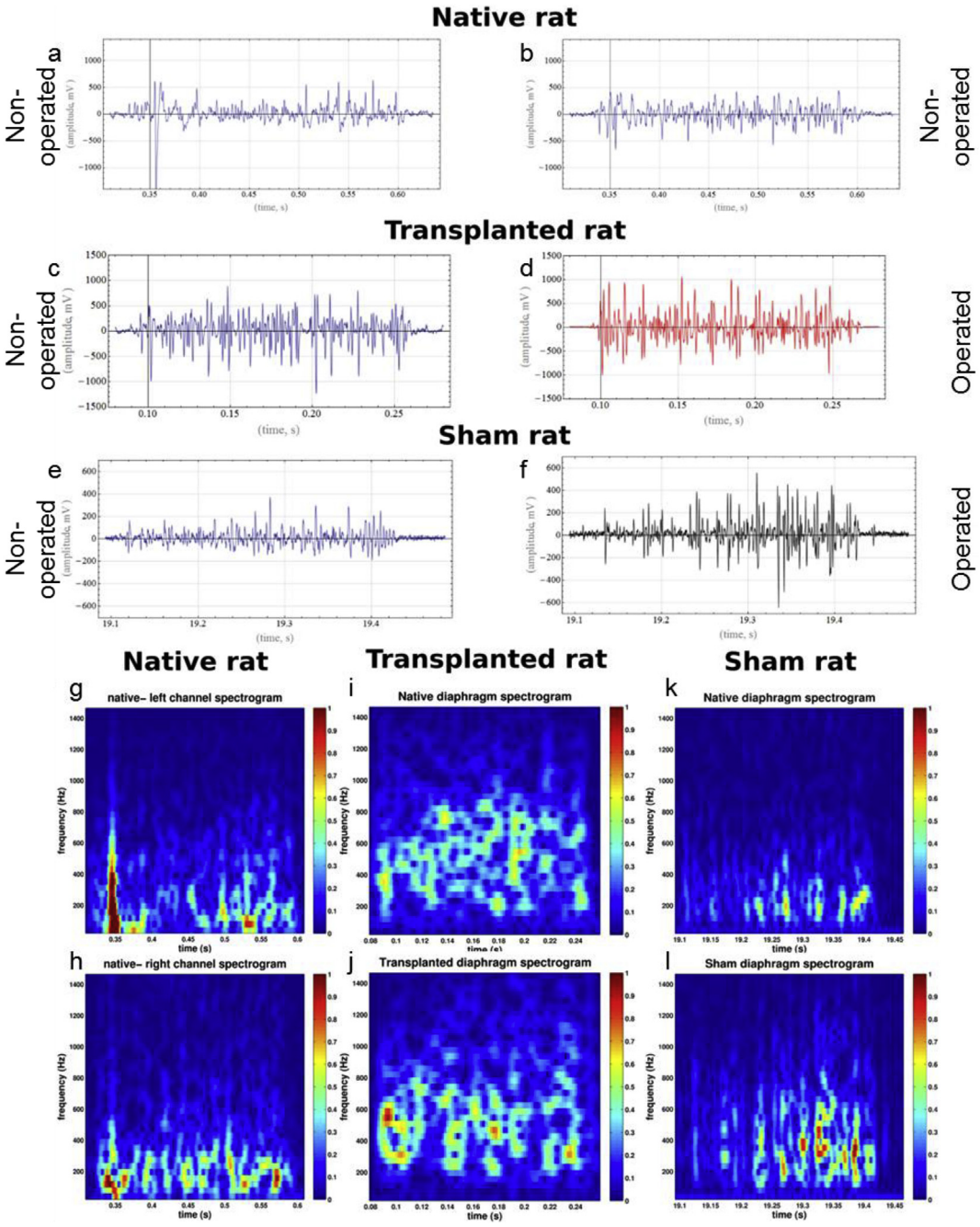

Fig. 8. Electromyography (EMG) after 21 days. (**a**–**f**) Typical waveforms of single contractions of left and right diaphragms' dome of (**a**, **b**) native, (**c**, **d**) transplanted and (**e**, **f**) sham rats. (**g**–**l**) EMG spectrograms (left and right diaphragms' dome) of (**g**, **h**) native, (**i**, **j**) transplanted and (**k**, **l**) sham rats. For the purposes of comparing the spectrograms of each dome, the spectral values were normalized using the maximum spectral value from both spectrograms. Most of the signal is concentrated below 1000 Hz.

a critical time when biological tissue engineered scaffolds typically fail resulting in reherniations. After 21 days in an orthotopic position, the scaffold was completely re-populated with cells, suggesting that the blood supply was sufficient to support nascent, functioning cells. Macroscopic proof of *neo*-vascularization was confirmed by H&E staining and immunostaining for VEGF and vWF. Based on these results, essential microcirculation was achieved after transplantation of the recellularized diaphragmatic graft.

The ultimate goal of any tissue engineered organ transplantation is restoration and maintenance of the native organ's function. For the diaphragm, this includes restoration of innervation and an intact muscle contraction in response to these nerve signals. Initial *in vitro* testing for calcium transients in the reseeded cells, after 3 weeks of culture on a decellularized scaffold, was negative (data not shown). Despite this result, functional contractile properties appeared to have been restored after transplantation, as evidenced by pulmonary function evaluations of the transplanted animals and EMG testing *in situ*. Two hypotheses exist to explain the difference between the observations of *in vitro* and *in vivo* assessment. The reseeded cells may require more tissue specific signals than in the *in vitro* setting to express voltage dependent channels and the specialized calcium machinery characteristic of a muscle cell [31], which they receive *in vivo*; or *in vivo* the scaffold is gradually repopulated with the recipient's cells, or a

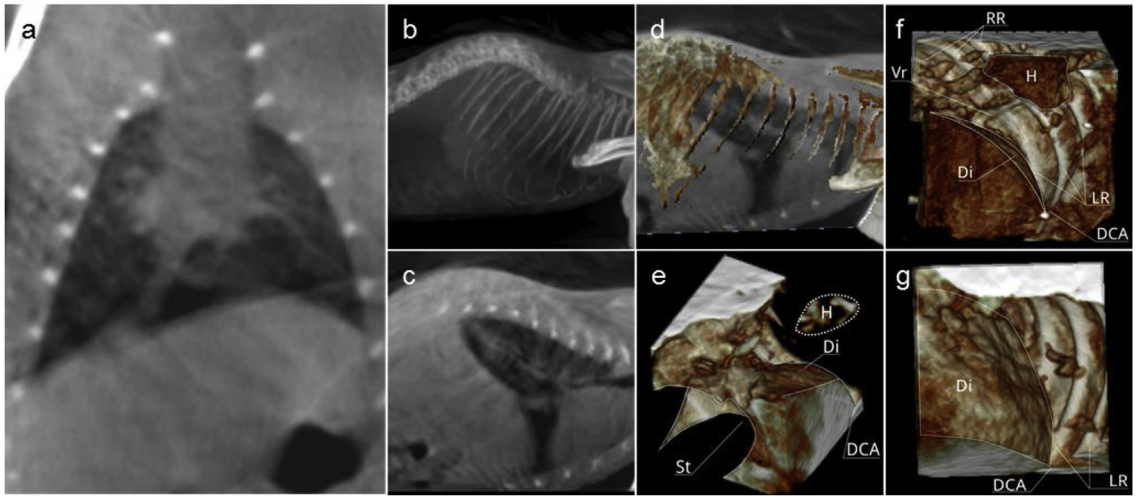

Fig. 9. Computed tomography of transplanted rat. (**a**–**g**) Computed tomography. Multi planar reconstruction: (**a**) frontal view, (**b**, **c**) coronal view. (**d**–**g**) Volume rendering (**RR** – right ribs, **LR** – left ribs, **Di** – diaphragm, **H** – heart, **DCA** – diaphragmatic-costal angle, **ST** – stomach, **Vr** – vertebra).

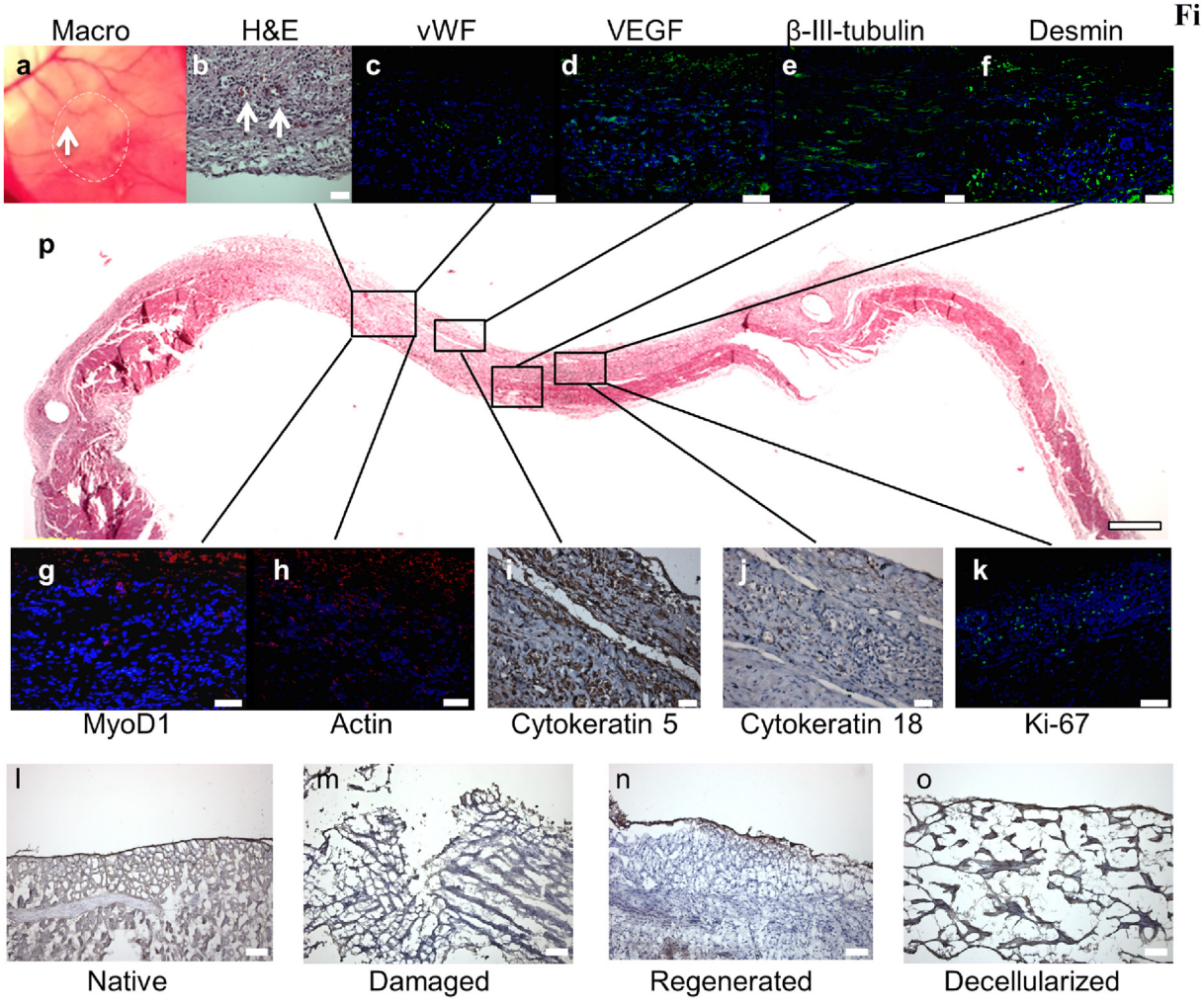

Fig. 10. Twenty one-day post-orthotopic transplantation. (**a**) Macroscopic image of orthotopic replacement of the left hemi-diaphragm with a reseeded tissue engineered graft (dashed line – transplant, arrow – newly formed vessel). (**b**) Magnified H&E sections show several blood vessels and positive staining for vWF (**c**) and VEGF (**d**). Repopulation of the scaffold by different cell types was demonstrated by immunohistochemistry: β-III-tubulin-positive staining (**e**) suggestive of in-growth of neurons, desmin-positive (**f**), MyoD1-positive (**g**) and actin-positive (**h**) cells were found throughout the graft. The neo-mesothelium stained positively for cytokeratin 5 (**i**) and 18 (**j**). Proliferative cells were found in all layers of diaphragm transplant (**k**). (Scale bar – 20 μm). We used biotin assay in order to functionally test the regenerated epithelium; the native epithelium showed superficial staining (brown color) (**l**), while a mechanically damaged tissue (control) demonstrated deeper staining (**m**). The regenerated epithelium (**n**) appeared similar to the native layer. The decellularized scaffold staining demonstrated general diffusion into the tissue (**o**) suggesting some deficit in the epithelium layer (scale bar – 50 μm). (**p**) H&E overview of *in vivo* regenerated diaphragm (scale bar – 200 μm). (For interpretation of the references to color in this figure legend, the reader is referred to the web version of this article.)

combination of the two. Although the ECM provides an *in vitro* microenvironment that allows cell attachment and proliferation [37], it clearly is not currently capable of completing the regeneration of functional organ without *in vivo* factors. Further studies are necessary to evaluate the *in vivo vs. in vitro* functionality of the reseeded construct.

Two findings of recovered muscle functionality of the tissue engineered diaphragms were observed *in vivo*. The first was pulmonary function testing which revealed a flow/volume curve similar to that of unaltered rats. This finding requires both adequate innervation of the diaphragm and intact muscle response and contraction. Interestingly, the functional results of transplanted, sham and native rats were similar. The analysis of the full EMG sequence revealed that electrical activity on both hemi-diaphragms of the transplanted and native rats started simultaneously, however in the sham group the operated hemi-diaphragm showed a time lag compared to the intact one (as indicated by the time lag analyses in Table 2). This could indicate that the source electrical activity in the host tissue propagates passively, or with a reduced conduction velocity, into the implanted dome. Whereas the simultaneous start of electrical activity on both halves of the diaphragm in the transplanted group suggests functional reinnervation. Further investigation is necessary to prove this, however neuromuscular junction reformation after muscle injury is uncommon. Blood gas analyses also indicated equal and adequate end respiratory function of the tissue engineered diaphragm and its native counterpart – further suggesting full integration of the graft.

Another key property of a fully restored and functional bioengineered diaphragm is maintenance of the impervious barrier between the chest and abdominal cavities. Equal diaphragmatic excursion of the left and right hemi-diaphragms on CT and X-ray images indicate the preservation of anatomical integrity of the tissue engineered transplant, free from structural and mobility defects. The restoration of barrier function was proven by lack of pneumothoraces, normal heart axis location, and an absence of protrusions or eventrations detectable by CT and X-ray examinations. Further, the regenerated diaphragm was covered by mesothelium, which was confirmed with biotin assay testing.

5. Conclusion

We have developed an optimized decellularization protocol for rat diaphragms based on our previously described detergent-enzymatic method [26], to obtain a biological scaffold for diaphragm replacement. The scaffold maintained structural integrity and essential biomechanical properties, was non-immunogenic and stimulated angiogenesis. Successful scaffold recellularization was performed with rat BM-MSCs before being transplanted into an orthotopic position for 21 days in a small animal model. The cells, in combination with bioactive molecules from the scaffold, help to direct the organotypic regeneration rather than scar tissue formation. The tissue engineered rat diaphragms remained non-immunogenic *in vivo*, therefore potentially harmful immunosuppression was not necessary. The bioengineered diaphragms maintained functional respiratory homeostasis without evidence of complications. This study represents the first pre-clinical evidence of successful transplantations of decellularized diaphragms seeded with allogeneic rat MSCs with restoration of essential functional properties after replacement of 80% of the left hemi-diaphragm. Lessons learned from our group's successes with less complex tissue engineered hollow organs (tracheae and oesophagi) were used to create this functional, dynamic, durable and non-immunogenic diaphragmatic replacement. Its creation significantly advances complex tissue engineered organ replacements and represents an encouraging potential surgical treatment for patients with large diaphragmatic defects and limited therapeutic options. In light of these promising results, the future focus will be on replicating this study in a large animal model before attempting this in a clinical setting.

Competing financial interests

The authors indicate no potential competing financial interests.

Acknowledgments

We would like to thank Kirill Labunets and Alexander Gubarev for 3D-bioreactor model construction. Also we would like to thank Korovashkin S.A., Cherchenko A.V., Minosyan K.E. (State Institution of Health «Regional Clinical Dental Clinic», Krasnodar, Russian Federation) for assistance with the CT studies and Alexander Atoyantz (Department of Human Physiology, Kuban State Medical University, Krasnodar, Russia) for assistance with EMG studies. This study was supported and financed by Bioengineering of Tracheal Tissue and the Government of the Russian Federation Grant (Agreement No. 11.G34.31.0065).

Appendix A. Supplementary data

Supplementary data related to this article can be found at http://dx.doi.org/10.1016/j.biomaterials.2015.11.020.

References

[1] A.J. Merrell, G. Kardon, Development of the diaphragm – a skeletal muscle essential for mammalian respiration [Internet], FEBS J. 280 (17) (2013) 4026–4035.
[2] S. Mayer, R. Metzger, D. Kluth, The embryology of the diaphragm, Semin. Pediatr. Surg. 20 (3) (2011) 161–169.
[3] J.W. Logan, H.E. Rice, R.N. Goldberg, C.M. Cotten, Congenital diaphragmatic hernia: a systematic review and summary of best-evidence practice strategies, J. Perinatol. 27 (9) (2007) 535–549.
[4] C.A. Laituri, et al., Outcome of congenital diaphragmatic hernia repair depending on patch type [Internet], Eur. J. Pediatr. Surg. 20 (6) (2010) 363–365.
[5] J. Haroon, R.S. Chamberlain, An evidence-based review of the current treatment of congenital diaphragmatic hernia, Clin. Pediatr. (Phila). 52 (2) (2013) 115–124.
[6] L. Leeuwen, D.A. Fitzgerald, Congenital diaphragmatic hernia, J. Paediatr. Child. Health 50 (9) (2014) 667–673.
[7] A.R.R. Lima, et al., Heart failure-induced diaphragm myopathy, Cell. Physiol. Biochem. 34 (2) (2014) 333–345.
[8] M.S. Maish, The diaphragm, Surg. Clin. N. Am. 90 (5) (2010) 955–968.
[9] K. Turhan, et al., Traumatic diaphragmatic rupture: look to see, Eur. J. Cardiothorac. Surg. 33 (6) (2008) 1082–1085.
[10] M.P. Kim, W.L. Hofstetter, Tumors of the diaphragm, Thorac. Surg. Clin. 19 (4) (2009) 521–529.
[11] E. Chan, C. Wayne, A. Nasr, Minimally invasive versus open repair of Bochdalek hernia: a meta-analysis, J. Pediatr. Surg. 49 (5) (2014) 694–699.
[12] S. Thapar, A. Ahuja, A. Rastogi, Rare diaphragmatic tumor mimicking liver mass, World J. Gastrointest. Surg. 6 (2) (2014) 33–37.
[13] K.B. Ricci, V.C. Daniel, C. Sai-Sudhakar, R. Higgins, Bovine pericardium diaphragm repair of diaphragmatic hernia after LVAD explantation and heart transplantation, Am. J. Transpl. 14 (8) (2014) 1941–1943.
[14] S. Loff, et al., Implantation of a cone-shaped double-fixed patch increases abdominal space and prevents recurrence of large defects in congenital diaphragmatic hernia, J. Pediatr. Surg. 40 (11) (2005) 1701–1705.
[15] I.C. Mitchell, et al., Permacol: a potential biologic patch alternative in congenital diaphragmatic hernia repair, J. Pediatr. Surg. 43 (12) (2008) 2161–2164.
[16] J.A. Sandoval, et al., The whole truth: comparative analysis of diaphragmatic hernia repair using 4-ply vs 8-ply small intestinal submucosa in a growing animal model, J. Pediatr. Surg. 41 (3) (2006) 518–523.
[17] K. Tsao, K.P. Lally, Innovations in the surgical management of congenital diaphragmatic hernia, Clin. Perinatol. 39 (2) (2012) 363–374.
[18] W. Zhao, et al., Diaphragmatic muscle reconstruction with an aligned electrospun poly(ε-caprolactone)/collagen hybrid scaffold, Biomaterials 34 (33) (2013) 8235–8240.
[19] K. Masumoto, et al., Effectiveness of diaphragmatic repair using an abdominal muscle flap in patients with recurrent congenital diaphragmatic hernia, J. Pediatr. Surg. 42 (12) (2007) 2007–2011.

[20] M.T. Conconi, et al., Homologous muscle acellular matrix seeded with autologous myoblasts as a tissue-engineering approach to abdominal wall-defect repair, Biomaterials 26 (15) (2005) 2567–2574.
[21] J. Haag, et al., Biomechanical and angiogenic properties of tissue-engineered rat trachea using genipin cross-linked decellularized tissue, Biomaterials 33 (3) (2012) 780–789.
[22] P. Jungebluth, et al., Structural and morphologic evaluation of a novel detergent-enzymatic tissue-engineered tracheal tubular matrix, J. Thorac. Cardiovasc. Surg. 138 (3) (2009) 583–586.
[23] P. Macchiarini, et al., Clinical transplantation of a tissue-engineered airway, Lancet 372 (9655) (2008) 2023–2030.
[24] A. Gonfiotti, et al., The first tissue-engineered airway transplantation: 5-year follow-up results, Lancet 383 (9913) (2014) 238–244.
[25] S. Sjöqvist, et al., Experimental orthotopic transplantation of a tissue-engineered oesophagus in rats, Nat. Commun. 5 (2014), http://dx.doi.org/10.1038/ncomms4562.
[26] E.A. Gubareva, A. Sotnichenko, I. Gilevich, P. Macchiarini, Optimal decellularization of rat hearts and diaphragms and morphological evaluation, Cell. Transplant. Tissue Eng. 7 (4) (2012) 38–45.
[27] P. Macchiarini, E. Kondratieva, Features of ethical expertise in planning and conducting clinical research in regenerative medicine, Cell. Transplant. Tissue Eng. 74 (2011) 111–114.
[28] Y. Gustafsson, et al., Viability and proliferation of rat MSCs on adhesion protein-modified PET and PU scaffolds, Biomaterials 33 (32) (2012) 8094–8103.
[29] S.G. Sotocinal, et al., The Rat Grimace Scale: a partially automated method for quantifying pain in the laboratory rat via facial expressions, Mol. Pain 7 (2011) 55.
[30] J. Shimazaki, K. Higa, N. Kato, Y. Satake, Barrier function of cultivated limbal and oral mucosal epithelial cell sheets, Investig. Ophthalmol. Vis. Sci. 50 (12) (2009) 5672–5680.
[31] M.J. Berridge, M.D. Bootman, H.L. Roderick, Calcium signalling: dynamics, homeostasis and remodelling, Nat. Rev. Mol. Cell Biol. 4 (7) (2003) 517–529.
[32] T.M. Macleod, G. Williams, R. Sanders, C.J. Green, Histological evaluation of Permacol as a subcutaneous implant over a 20-week period in the rat model, Br. J. Plast. Surg. 58 (4) (2005) 518–532.
[33] L. Wen, et al., Immunomodulatory effects of bone marrow-derived mesenchymal stem cells on pro-inflammatory cytokine-stimulated human corneal epithelial cells, PLoS One 9 (7) (2014) e101841.
[34] P. Jungebluth, P. Macchiarini, Airway transplantation, Thorac. Surg. Clin. 24 (1) (2014) 97–106.
[35] D.A. Taylor, From stem cells and cadaveric matrix to engineered organs, Curr. Opin. Biotechnol. 20 (5) (2009) 598–605.
[36] N.A. Andreollo, E.F. dos Santos, M.R. Araújo, L.R. Lopes, Rat's age versus human's age: what is the relationship? Arq. Bras. Cir. Dig. 25 (1) (2012) 49–51.
[37] M.T. Wolf, C.L. Dearth, S.B. Sonnenberg, E.G. Loboa, S.F. Badylak, Naturally derived and synthetic scaffolds for skeletal muscle reconstruction, Adv. Drug Deliv. Rev. 84 (2015) 208–221, http://dx.doi.org/10.1016/j.addr.2014.08.011.
[38] G. Lemon, et al., The use of mathematical modelling for improving the tissue engineering of organs and stem cell therapy, Curr. Stem Cell Res. Ther. (2015) [published online ahead of print: October 1, 2015].